Folding Kinetics of the Protein Pectate Lyase C Reveal Fast-Forming Intermediates and Slow Proline Isomerization[†,‡]

Douglas E. Kamen[§] and Robert W. Woody*

Department of Biochemistry and Molecular Biology, Colorado State University, Fort Collins, Colorado 80523

Received July 19, 2001; Revised Manuscript Received February 8, 2002

ABSTRACT: Pectate lyase C (pelC) is a member of the class of proteins that possess a parallel β-helix folding motif. A study of the kinetic folding mechanism is presented in this report. Kinetic circular dichroism (CD) and fluorescence have been used to observe changes in the structure of pelC as a function of time upon folding and unfolding. Three folding phases are observed with far-UV CD and four phases are observed with near-UV CD. The two slowest phases have relaxation times on the order of 21 and 46 s in aqueous buffer. Double-jump refolding assays and the measured activation enthalpies (16.0 and 21.2 kcal/mol for the respective slow phases) suggest that these two phases are the result of the slow *cis*−*trans* isomerization of prolyl-peptide bonds. We have determined that the earliest observed folding phase involves the formation of most, if not all, of the secondary structure with a relaxation time of 0.25 s. We also observed a phase by near-UV CD on the order of 0.25 s. This suggests that along with the appearance of secondary structure, some tertiary contacts are made. There is one kinetic phase observed in the near-UV CD and fluorescence that has no corresponding far-UV CD phase. This occurs with a relaxation time of 1.1 s. The temperature dependence of the natural log of the folding rate constant suggests that folding occurs via a sequential mechanism in which an on-pathway intermediate in rapid equilibrium with the unfolded protein is present. Semiempirical CD calculations support the idea that the β-helix region of pelC forms in the fast kinetic phase, yielding near-native secondary and tertiary structures in that region. This is followed by the slower formation of the loop regions connecting individual strands of the β-helix.

In recent years, significant advances in the field of protein folding have been made. These advances have come in the form of insightful theoretical models (*1*−*3*) and information-rich experimental advances (*4*−*6*). Protein folding is currently viewed from the perspective of free energy surfaces in which the delicate balance between enthalpy and entropy contribute to guide an unfolded polypeptide chain along a free-energy surface toward the native, active biological entity. Developments and advances in instrumentation and techniques have led to observation of folding reactions in the milli-, micro-, and nanosecond time scales (*7*−*12*). These achievements over the last several years have led to a shift in the way one thinks about protein folding (*1*) and a deeper understanding of the physical phenomenon of folding.

Small, single-domain proteins that fold via a two-state mechanism have been the focus of many recent studies (*13*−*16*). These studies have provided much of the basis for understanding the fundamental properties of protein folding. In this paper, an initial characterization of the folding kinetics of pectate lyase C (pelC)[1] from *Erwinia chrysanthemi* is presented. PelC is a member of the class of proteins containing a parallel β-helix folding motif (*17*, *18*). It was the first protein observed to possess such a backbone topology (*18*). The majority of the regular secondary structure is composed of parallel β-sheets (about 30%). The individual strands of the sheets are connected by unordered loops of varying length (Figure 1). The architecture of the sheets results in the backbone winding up to form a large helix composed of β-sheets. There are two disulfide bonds in pelC that remain intact throughout all of the experiments reported here. In addition, there are 12 proline residues. One of these prolines, Pro220, is involved in a *cis* peptide bond (*18*).

The in vitro folding of this class of proteins has been largely untouched. Several studies on the in vivo folding, misfolding and assembly of the tailspike protein from bacteriophage P22 have been published (*19*−*22*). In addition, some in vitro work has been done on the tailspike protein (*23*, *24*). We propose that because of the relatively simple topology of the parallel β-helix, these proteins will be excellent folding models, yielding relatively simple and easily understood mechanisms. It is also important to understand the nature of the folding of these proteins because amyloid fibrils may be assembled from β-helical precursors (*25*).

This study represents a detailed characterization of the in vitro kinetic folding mechanism of a parallel β-helix protein. Evidence is presented that indicates that the slow *cis*−*trans*

[†] Supported by USPHS Grant GM-22994.

[‡] From a dissertation submitted to the Academic Faculty of Colorado State University in partial fulfillment of the requirements for the degree of Doctor of Philosophy.

* To whom correspondence should be addressed. E-mail: rww@lamar.colostate.edu. Fax: (970) 491-0494.

[§] Current address: Department of Biochemistry, Albert Einstein College of Medicine, Bronx, NY 10461.

[1] Abbreviations: CD, circular dichroism; gdn-HCl, guanidine-hydrochloride; LB, Luria-Bertani; MES, 2-[*N*-morpholino]ethanesulfonic acid; pelC, pectate lyase C; PPI, peptidyl-prolyl isomerase; WT, wild-type. Standard abbreviations are used for the amino acids and nucleic acid bases.

10.1021/bi0115129 CCC: $22.00
Published on Web 03/15/2002

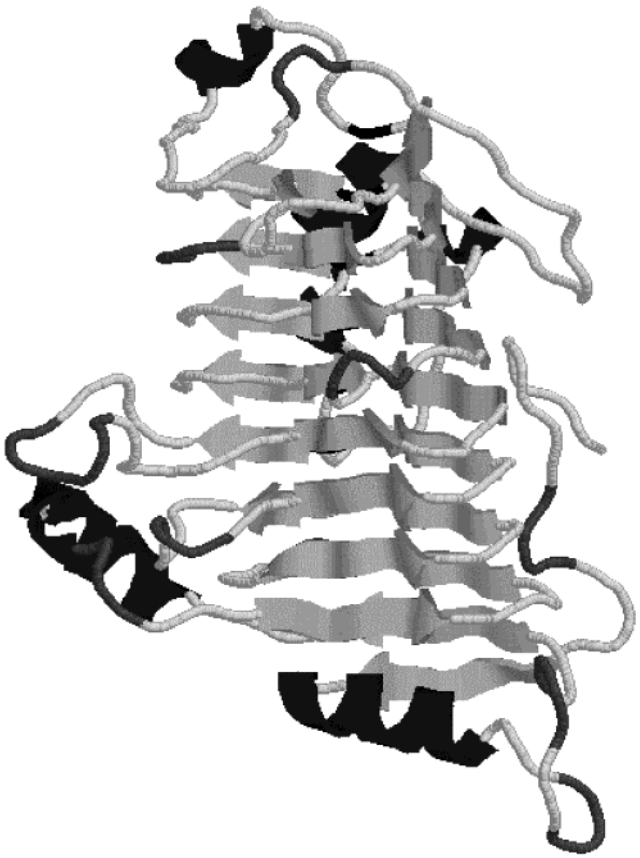

FIGURE 1: A model of the structure of pelC determined by X-ray crystallography (*17*). β-Sheets are shown as gray arrows, and α-helixes are shown as black coils. This image was generated using RasMol (*64*).

isomerization around X-Pro peptide bonds is a major event in the folding of pelC. Two slow kinetic phases have been assigned to proline isomerization. One fast folding phase is also observed that corresponds to the rapid and highly cooperative formation of the secondary structure. There are two kinetic phases that have been assigned to the formation of ordered side-chain structure. Semiempirical calculations were used to calculate the CD spectrum of pelC and pelC with deleted aromatic side chains. Results from the calculations support a model in which the β-helix region of pelC folds in the fast kinetic phase. The formation of the loop regions occurs in a subsequent slower step that is dependent on the formation of the β-helix region. A folding model of pelC is presented. With the exception of complications arising from proline isomerization, the model presented is relatively simple, consistent with the simple topology of the parallel β-helix.

MATERIAL AND METHODS

Materials. All chemicals purchased were of the highest quality and purity. MES (2-[*N*-morpholino]ethanesulfonic acid) was >99.5% pure and purchased from Sigma Chemicals (St. Louis, MO). Ultrapure guanidine-hydrochloride (gdn-HCl) was purchased from ICN Biomedicals (Aurora, OH). Sodium chloride (99.9%) was purchased from Fisher Chemicals (Fair Lawn, NJ). PelC was prepared as previously described (*26*). Gel electrophoresis in sodium dodecyl sulfate gave a single band at the loadings used (ca. 10 μg). This shows that the purity of the protein was >98%.

Unfolding Kinetics. Unfolding of pelC was initiated by manually diluting a stock solution of pelC into a concentrated solution of gdn-HCl in a cuvette thermostated at 25 °C. The dead-time for this procedure was between 15 and 20 s. Unfolding was monitored by CD at 218 nm using a Jasco J-720 CD spectropolarimeter (Tokyo, Japan). A 0.1-cm path-length cell was employed for all measurements. The temperature of the cell was maintained by circulating water from a NES-LAB RTE 110 water bath. PelC concentrations were 5−10 μM. Kinetic traces utilized the following parameters: 0.5−1 s time resolution, 0.5−1 s response time, and a spectral bandwidth of 2.0 nm. Solution conditions were 25 mM MES, 15 mM NaCl, pH 6, and 1.0−5.0 M gdn-HCl. All kinetic experiments were fit to the following model:

$$\theta = \sum_{i=1}^{n} a_i \exp(-k_i t) + c \qquad (1)$$

θ is an observable parameter (CD, fluorescence,...), a_i is the amplitude of the *i*th phase, k_i is the rate constant of the *i*th phase, t is the time, and c is the equilibrium value of the observed property. All kinetic data were analyzed by nonlinear regression using the data analysis software Axum (MathSoft Inc, Northhampton, MA). This program uses the Levenberg-Marquardt (*27*) nonlinear least-squares algorithm to fit the curves. The reported errors represent the standard deviation of the mean, unless otherwise specified.

Folding Kinetics. The folding of pelC was initiated by either manual mixing or the stopped-flow technique. For manual-mixing experiments, a mixing device similar to that used by Kuwajima et al. (*28*) was employed. A rectangular cuvette holder was made. The holder was designed so that coolant could be circulated to regulate the temperature. In addition, a magnetic stirring device was installed (Starna Cells, Atascadero, CA). The result was a thermostated cuvette holder capable of holding a 1-cm path-length cell with a rotating stir bar inside. Dead times for this device were determined by measuring the time to mix a solution of 0.1% (+)-pantoyl lactone in 5 M gdn-HCl, 25 mM MES into 25 mM MES. The CD at 220 nm was followed as a function of time. The time it took for the CD signal to reach a constant value was taken as the mixing time. In all cases, additional time was allowed for the instrument response. The resulting dead-time was 4 s. In cases of high denaturant concentration or low temperature, when the folding is slow, a resolution of 5 s with a 4-s response time was used. PelC concentrations were 1 μM in 5 mM MES, 50 mM NaCl for data collected at 218 nm. CD in the near-UV was observed at 277 nm using a pelC concentration of 5μM.

To observe the earliest phases of the folding process, stopped-flow mixing was used. A Bio-Logic SFM-3 stopped-flow module (Claix, France) was interfaced with a Jasco J-720 CD spectropolarimeter. The stopped-flow device was equipped with a high-density solution mixer and a small-volume syringe for the sample. Solutions of pelC in 5 M gdn-HCl, 25 mM MES, 50 mM NaCl, pH 6, were equilibrated to 25 °C in the reservoir of the stopped-flow device. Dilutions were made into identically buffered solutions containing the necessary concentration of gdn-HCl in order to give the desired final gdn-HCl concentrations by a 50-fold dilution. A 0.2- or 1-cm flow cell was employed. Dead-

times were 12 ms. Data were collected at 20 ms intervals with a response time of 16 ms and a bandwidth of 2.0 nm. A total of 25−30 transients were averaged. For all CD measurements, pelC concentrations of 5 μM were used.

Temperature Dependence of Folding. The temperature dependence of the rate constant was determined for the slow folding phases. Activation enthalpies ($\Delta H^{\ddagger}$) were calculated using Eyring's equation from absolute rate theory (*29*):

$$\ln(k_f/T) = \ln(k_B/h) + \Delta S_f^{\ddagger}/R - \Delta H_f^{\ddagger}/RT \qquad (2)$$

In the above equation, k_f is the folding rate constant, T is the absolute temperature in Kelvin, k_B is Boltzmann's constant, h is Planck's constant, $\Delta S_f^{\ddagger}$ and $\Delta H_f^{\ddagger}$ are the transition state entropy and enthalpy changes for folding, respectively, and R is the gas constant. The folding rate constants for the slowest phase were measured with far-UV CD. Folding was measured in gdn-HCl concentrations of 0.1−0.4 M at temperatures from 5 to 25 °C. The activation enthalpy was determined for this phase using the extrapolated rates in 0 M gdn-HCl at each temperature. These rates were fit to eq 2, yielding activation parameters for folding. The activation enthalpy for the intermediate slow phase was obtained using the P220A mutant, as described in the following paper in this issue (*30*). Fluorescence emission spectroscopy was used to monitor folding following a jump in the pH from 2 to 6.

Double-Jump Folding Assay. Double-jump assays to test for the presence of slowly unfolding populations were performed for the slow phases of pelC folding. For the slowest phase, CD and fluorescence spectroscopies were used. PelC was unfolded in 5 M gdn-HCl in 25 mM pH 9.5 Gly-NaOH at 0 °C. Refolding was initiated after various delay times by 50-fold dilution of the unfolded pelC solution into 25 mM pH 6 MES, 50 mM NaCl at 25 °C and gdn-HCl necessary to make the final denaturant concentration 0.4 M. The final concentration of pelC was 1 μM. A 1-cm path-length cell was used. Refolding amplitudes were determined by fits of the data to eq 1. For the intermediate phase, only fluorescence was used because this method yielded better signal-to-noise ratios.

Folding Catalyzed by Peptidyl-Prolyl Isomerase. Human peptidyl-prolyl isomerase (also known as PPI or cyclophilin) was purchased from Sigma Chemical Co. (St. Louis, MO). Because the activity of PPI is significantly reduced in solutions containing gdn-HCl, folding was carried out by dilution of pelC unfolded in 9 M urea at pH 8.0 (50 mM Tris) to 0.3 M urea. Folding was followed by fluorescence emission spectroscopy. A final PPI concentration of 1 μM was used and included in the refolding buffer.

Semiempirical CD Calculations. Calculations were performed as described by Woody and Sreerama (*31*). The matrix method (*32*) in its origin-independent form (*33*) was used. The calculations consider three peptide transitions: nπ^*, $\pi\pi^*$ (NV_1), and $\pi\pi^*$ (NV_2). Transition moment directions for the secondary amide of *N*-acetylglycine were used for the $\pi\pi^*$ transitions (*34*). Transition monopole charges for the nπ^* transition and for transitions connecting the $\pi\pi^*$ and nπ^* excited states were calculated from INDO/S wave functions (*35*) for *N*-methylacetamide. The ground-state monopole charges were from Woody (*36*). Side-chain transitions of Trp and Tyr were included using the parameters described by Grishina and Woody (*37*). The monopole charges were located at atomic centers for aromatic side chains and at the positions given by the semiempirical Z values for amide transitions (*36*).

RESULTS

Unfolding Kinetics of pelC. Unfolding of pelC was monitored by far-UV CD. In all cases examined, the unfolding kinetics fit to a single-exponential model (Figure 2a). This suggests that unfolding is composed of a single process. Previous studies of the denaturation of pelC at equilibrium suggested that two unfolding units are present (*26*). This is not observed in the kinetic unfolding experiments, perhaps because the thermodynamic stabilities of the unfolding units are similar, or because the thermodynamic driving force for unfolding is so great that the two phases are not resolved. One interesting observation is made, however. The dependence of ln k_u on denaturant is nonlinear (Figure 3a). Similar observations have previously been interpreted as reflecting a change in the structure of the transition state with a change in denaturant concentration (*38*−*41*).

Folding Kinetics of pelC. The folding kinetics of pelC can be broken down into two parts, which include fast and slow phases. Stopped-flow CD was used to observe the fast-folding events, and manual-mixing techniques were used to observe the slow phases. The CD at 218 nm (far-UV) is an excellent indication of the formation of β-sheet secondary structure. Figure 2b shows a representative folding experiment of pelC monitored by CD at 218 nm. Unfolded pelC in 5 M gdn-HCl was diluted to 0.2 M to initiate refolding. The folding process consists of three phases. The stopped-flow data (Figure 2b, inset) fit a single exponential in the earliest time points that are resolved (residuals not shown). This fastest phase,[2] comprising about 40% of the total amplitude, has a relaxation time in buffer of 0.25 ± 0.01 s (Figure 2b, inset). There is no evidence for a 1-s phase, as is observed in near-UV CD and fluorescence. The slower decay at long times in the stopped-flow CD signal is compatible with the two processes observed in the manual mixing experiments. These two slow phases have relaxation times of 21 ± 2 s and 46 ± 1 s. The residuals for a single-exponential fit to the manual mixing data (see Figure S.1, Supporting Information) demonstrate the need for two exponentials to accommodate the systematic deviations at short times. The total change in amplitude in the kinetics experiments (∼5100 deg cm^2/dmol) is in very good agreement with the change observed for the equilibrium unfolding transition (∼5500 deg cm^2/dmol from ref *26*). The difference in amplitude, if real, probably results from the unfolded polypeptide adjusting to changing solvent conditions upon dilution of the denaturant (*42*). Figure 3a shows the dependence of the natural logarithm of the rate constant on final denaturant concentration for folding and unfolding. Figure 3b shows the change in amplitude of each phase as a function of denaturant concentration. Experiments were

[2] Throughout this paper, each kinetic phase is named according to the time constant as measured by the method that gives the highest accuracy. (See Table 1 for a comparison of time constants and associated error estimates from the three spectroscopic parameters.) For the three phases detectable by far-UV CD, the time constant is most accurately determined by the kinetics of $[\theta]_{218}$. The fourth phase is referred to as the 1.1-s phase because this is the time constant determined by near-UV CD, which is more accurate than fluorescence in this case.

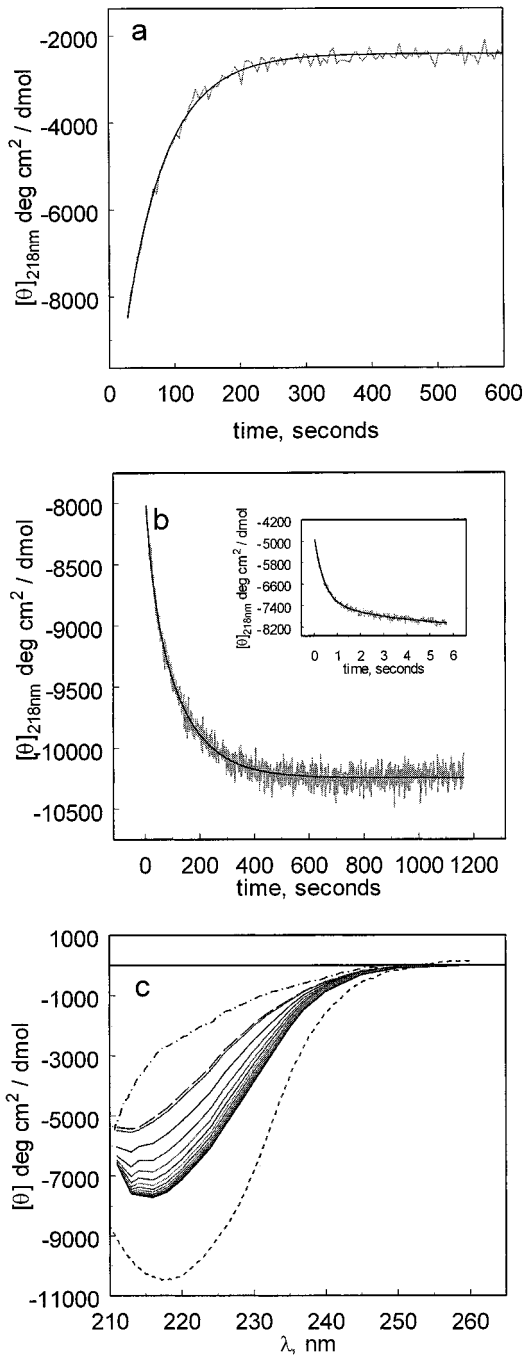

FIGURE 2: (a) A representative unfolding curve for pelC measured by far-UV CD in 5 M gdn-HCl, 25 mM MES and 50 mM NaCl at 25 °C. (b) A representative folding curve for pelC measured by far-UV CD. Conditions are 25 mM MES, pH 6, 50 mM NaCl, 0.2 M gdn-HCl, 25 °C. The main figure shows the results from manual mixing and the inset is from stopped-flow mixing. (c) Time-resolved CD spectra of the fast events in pelC folding. Final conditions were the same as *b*. Shown are the spectra of pelC in 5 M gdn-HCl (•-•-•), and native pelC (- - -). The solid lines are pelC folding from 0.24 to 2.2 s at 200 ms intervals. Also shown is the spectrum at 0 s determined by extrapolation (- − -).

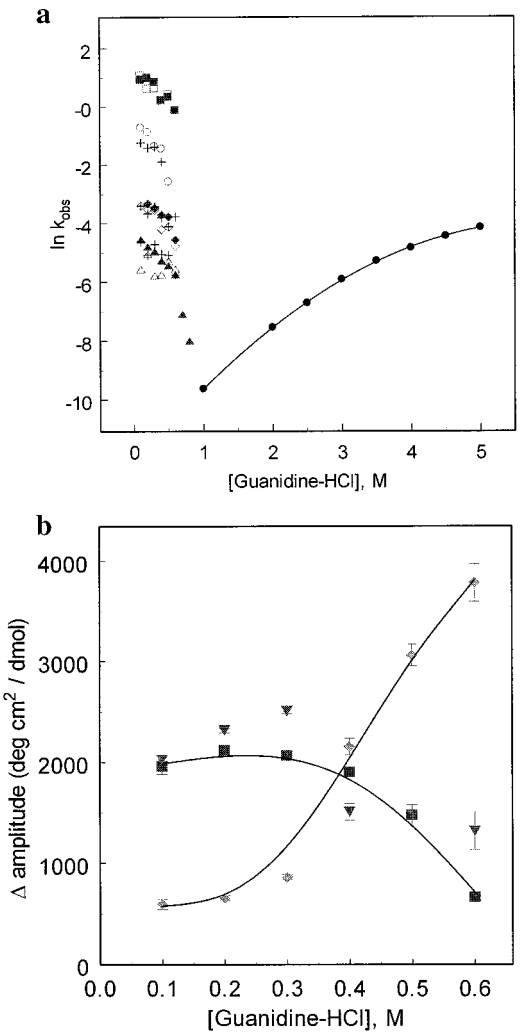

FIGURE 3: (a) natural log of the observed folding and unfolding rate constants as a function of final denaturant concentration. The filled circles are from unfolding experiments and are fit to a second-order polynomial [$\ln k_u = -12.2 + 2.8([\text{gdn-HCl}]) - 0.2([\text{gdn-HCl}])^2$]. The filled squares, diamonds and triangles represent the rate constants (k_{f1}, k_{f2}, and k_{f3} respectively) as determined by far-UV CD. The open symbols represent the respective rate constants as determined by near-UV CD. The open circles represent the phase observed by near-UV CD and not by far-UV CD. The plus signs represent the rate constants as determined by fluorescence. (b) The change in the folding amplitude determined by far-UV CD. The squares, diamonds and inverted triangles represent the measured amplitudes, a_{f1}, a_{f2}, and a_{f3} respectively. The solid lines are free-hand efforts to represent the trends in the data. Conditions are the same as outlined in Figure 2.

performed over a protein concentration range of 1−15 μM and no dependence of the rates or amplitudes on protein concentration was detected (data not shown). As the denaturant concentration is increased, the amplitude of the fast phase decreases, while the amplitude of the intermediate phase increases. The amplitude of the slowest phase shows little dependence on denaturant concentration. Figure 2c shows the time-resolved CD spectrum of the product of the fast phase. The spectrum is less intense, but the shape resembles that of a β-sheet-rich protein. This suggests that the intermediate has a very nativelike secondary structure.

The folding of pelC was also examined in the near-UV. CD at 277 nm is sensitive to the chiral environment of aromatic side chains. It is a good probe of the formation of tertiary structure. The folding process monitored at 277 nm has some interesting similarities and differences relative to that followed by 218 nm CD. A representative kinetic trace is shown in Figure 4a. One feature is the negative amplitude of the fastest phase (Figure 4a, inset). This is interesting for two reasons. The rate of this phase agrees, within experimental error, with that of the fast phase in the far-UV CD.

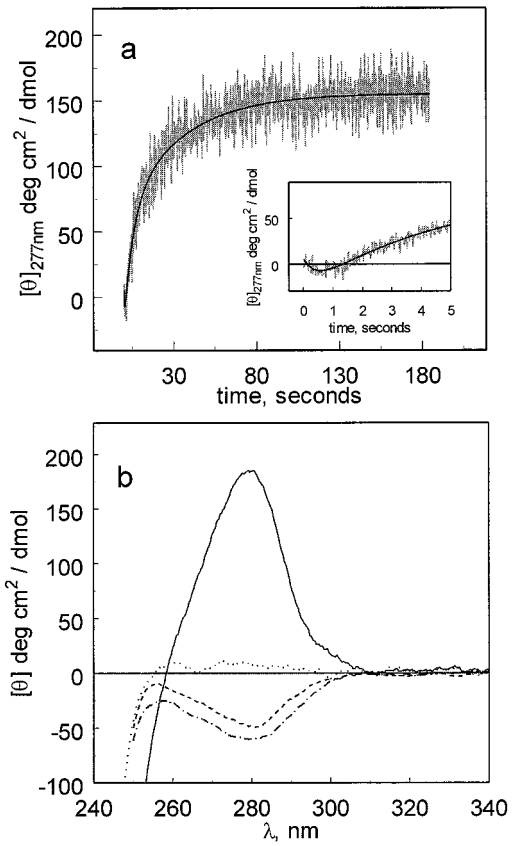

FIGURE 4: (a) A representative folding curve for pelC measured by near-UV CD at 277 nm. Conditions were 25 mM MES, 50 mM NaCl, 0.3 M gdn-HCl, 25 °C. The data are cut for clarity, but equilibrate to the native CD value. The inset shows the fast phase and the change in sign. (b) The equilibrium intermediate CD spectrum of pelC. Conditions are 25 mM gly-HCl pH 2, 25 °C, with no salt (···), 100 mM NaCl (- - -), 150 mM NaCl (•-•-•), and native pelC, pH 7 (−).

It is also opposite in sign to the native CD in the near-UV. There are two possible explanations for this observation. An intermediate is formed in the fast phase with nativelike secondary structure and nonnative tertiary structure, or the intermediate is nativelike and the aromatic residues that are structured make a negative contribution to the native CD spectrum, which overall is positive. The latter seems plausible due to the fact that at low pH, a salt-induced intermediate also has a negative sign for the CD in the near-UV (Figure 4b). It is also interesting in that there are four kinetic phases resolved in the near-UV (Figure 3a). The change in sign of the near-UV CD in the stopped-flow trace between 1s and 2s clearly indicates the need for two exponentials with time constants of seconds or less. This is borne out by the analysis (Table 1), which gives time constants of 0.33 ± 0.1 and 1.1 ± 0.1 s. The manual-mixing data (Figure 3a) also require two exponentials, as evidenced by a comparison of the residuals from a one- vs two-exponential fit (Figure S.4 Supporting Information). These longer time constants of about 25 ± 2 s and 75 ± 60 s (Table 1) also agree, within experimental error, with the two slower processes seen in the far-UV CD. Three of these near-UV CD phases have rates that correlate with the phases observed by far-UV CD, and one phase is unique (relaxation time = 1.1 ± 0.1 s). This indicates that the secondary structure forms very rapidly along with some tertiary structure, followed by the formation of the remainder of the tertiary structure. The 1.1-s phase may involve the folding of this intermediate to the native state.

Table 1: Relaxation Times and Amplitudes for Folding of pelC in 0 M Denaturant Concentration[a]

	far-UV CD	near-UV CD	fluorescence
τ_1	0.25 ± 0.01	0.33 ± 0.1	n.o.[c]
τ_2	nd[d]	1.1 ± 0.1	1.7 ± 0.6
τ_3	21 ± 2	25 ± 2	25 ± 2[b]
τ_4	46 ± 1	75 ± 60	83 ± 28
a_1	1960 ± 84	−35 ± 4	n.o.[c]
a_2	nd[d]	105 ± 9	0.24 ± 0.04
a_3	600 ± 31	60 ± 8	0.11 ± 0.01
a_4	2565 ± 150	25 ± 9	0.18 ± 0.01

[a] The relaxation times and amplitudes shown are those in 0 M denaturant, determined by extrapolation from the values measured at increasing denaturant concentration. Error estimates are based upon the mean error from a linear least-squares analysis. Because the extrapolation is for ln τ rather than τ, the error bounds on τ are asymmetric. However, the upper and lower values were averaged and reported here. Conditions are 25 °C, pH 6, 25 mM MES, 50 mM NaCl. The units for the relaxation times are seconds. The units for the folding amplitudes as measured by CD are deg cm^2/dmol, and for fluorescence the units are relative intensity. [b] In the following paper in this issue (*30*), the relaxation time for this phase was measured with a pH jump by fluorescence in the P220A mutant to be 21 s. This is probably a more accurate measurement than that obtained by extrapolation. [c] Not observable in manual-mixing experiments. [d] Not detected in far-UV CD.

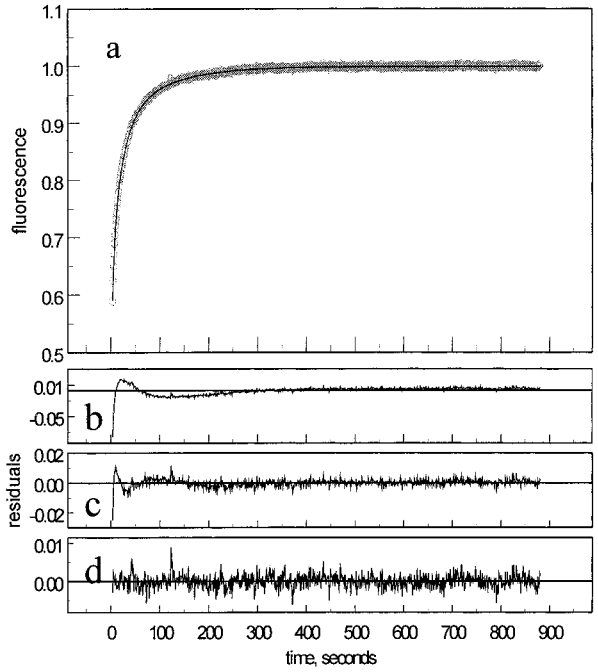

FIGURE 5: (a) Representative folding experiment for pelC monitored by fluorescence spectroscopy showing the slow-folding kinetics. Conditions are 0.3 M gdn-HCl, pH 6 MES 25 mM, 50 mM NaCl, 25 °C. The excitation wavelength was 290 nm and emission was followed at 326 nm. The data are fit to the sum of three exponentials. Residuals are shown for the single (b), double (c), and triple exponential fits (d).

Manual-mixing experiments were also monitored by fluorescence (Figure 5). Three exponentials are clearly needed to fit these data, as seen by a comparison of residuals obtained with one-, two-, and three-exponential fits. Only the latter shows residuals that exhibit no systematic deviations from zero. The time constants derived from fluorescence data are 1.7 ± 0.6 s, 25 ± 2 s, and 83 ± 28 s (Table

1), agreeing with those obtained from far- and near-UV CD, within allowable error. Although the mean time constants from far-UV CD and fluorescence differ by more than the sum of their estimated errors, Figure 3a shows that the far-UV CD data show substantially less scatter than the fluorescence data, and the extrapolation to zero denaturant concentration is therefore more reliable for the far-UV CD results. There is no evidence that different processes are being observed in far-UV CD and in fluorescence. On the contrary, the double-jump experiments described below provide evidence that the two spectroscopic probes are following the same slow process. It is interesting to note that the two spectroscopic probes that sense tertiary structure reveal the 1.1-s phase, whereas the far-UV CD that senses secondary structure does not exhibit this phase.

At high temperatures, and especially in gdn-HCl concentrations above 0.6 M, single-exponential kinetics are observed (Figures 6a and b). This suggests that at these extreme conditions, all the intermediates in the folding process are destabilized and no longer detectable, thus yielding two-state kinetics. Intermediates are still present under these conditions, but they are in rapid equilibrium with the unfolded state. Evidence for the presence of intermediates can be seen from the temperature dependence of the folding rate constant for the slowest phase (Figure 6c). For simple two-state processes, the rate constant must monotonically increase with temperature. At all gdn-HCl concentrations examined, the slow folding rate constant does not increase monotonically with temperature, but is maximal at a certain temperature. A model employing an on-pathway intermediate in rapid equilibrium with the unfolded state would display this non-Arhennius type of temperature dependence of the rate constants (*43*, *44)*. This suggests that the intermediate is necessary for folding and is populated to some degree under all conditions examined.

The Two Slow Steps of pelC Folding Are Due to Proline Isomerization. For many proteins, the slow kinetic phases have been shown to be the result of *cis*−*trans* isomerization about prolyl-peptide bonds (*45*−*48*). In model peptides, this isomerization occurs with a relaxation time of 10−100 s near room temperature (*45*). In the unfolded ensemble, the *trans* isomer of proline is more favorable than the *cis*, but in a folded protein, structural constraints can result in the stabilization of the *cis* isomer. This is somewhat common with X-Pro peptide bonds because the relative stability of the *trans* isomer is decreased. The equilibration of the isomers occurs relatively slowly due to a high enthalpic barrier. In pelC, the two slow phases have relaxation times in denaturant-free buffer of 21 and 46 s. It was therefore hypothesized that proline isomerization is occurring.

One way to test for the presence of proline isomerization is to use the double-jump technique. This procedure takes advantage of the fact that there is a high enthalpic barrier to proline isomerization relative to protein folding or unfolding. If the slow phases are due to a slow isomerization, such as prolyl-peptide bond isomerization, then the amplitudes of these phases will increase with increasing delay time. This is because at short delay times relatively few prolines will have undergone isomerization from the native conformation. As time goes by, equilibrium is reached and a stable population of incorrect isomers will be present. Figure 7 shows double-jump experiments using far-UV CD and

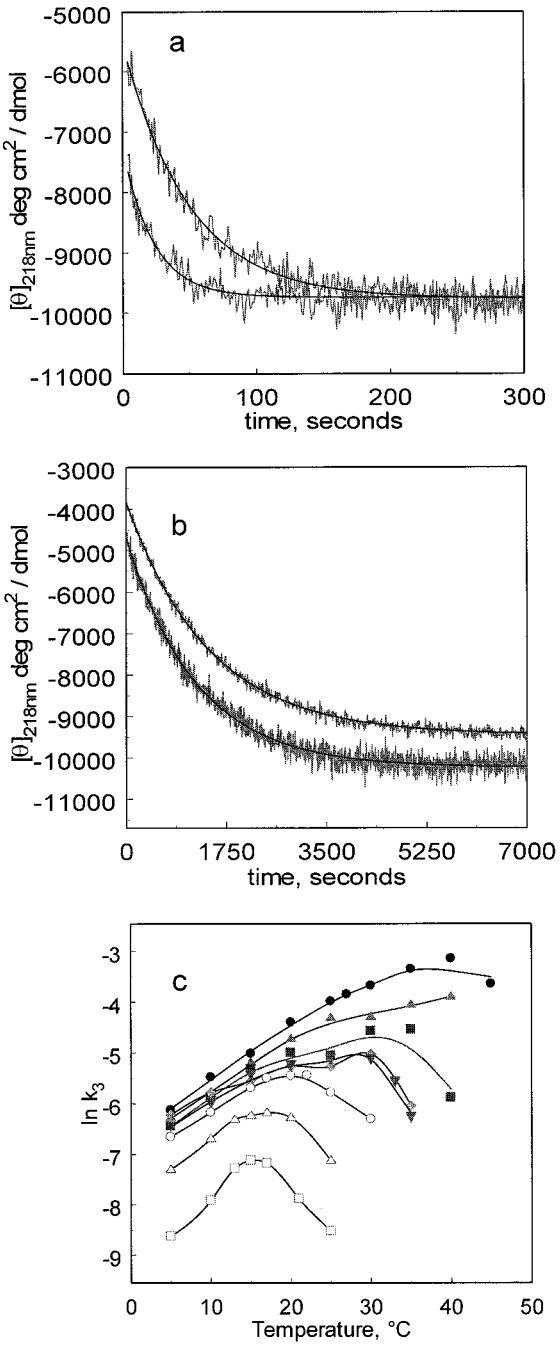

FIGURE 6: Folding kinetics measured by far-UV CD (218 nm) by manual mixing. (a) 0.1 and 0.2 M gdn-HCl at 40 °C and (b) 0.7 M gdn-HCl at 25 °C and 0.8 M gdn-HCl at 15 °C (bottom to top in both). Conditions were the same as from Figure 4. (c) The natural log of the rate constant for the slow folding phase at various denaturant concentrations (top to bottom: 0.1−0.8 M gdn-HCl) and temperatures (5°-45 °C). The solid lines are free-hand efforts to represent the trends in the data.

fluorescence. Using fluorescence spectroscopy, three kinetic folding phases are observed with rates consistent with those observed by CD (Figure 3a). This technique yielded much better signal-to-noise ratios and was therefore used for very precise determination of the relative amplitudes for the kinetic traces obtained at various delay times. It is demonstrated in Figure 7a that the relative change in amplitude for the slowest phase, as measured by CD and fluorescence, is identical. The overall results indicate behavior typical of proline isomerization. With increasing delay time, the relative

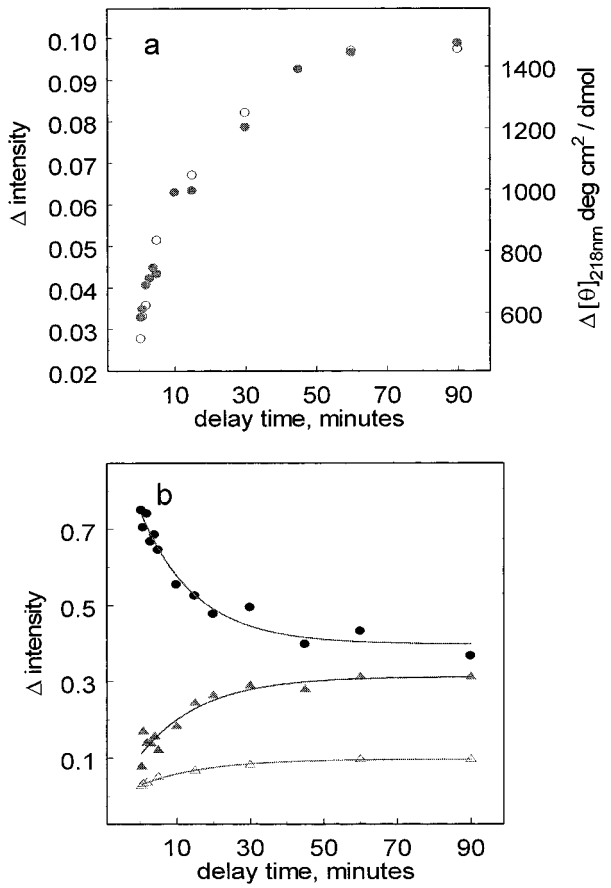

FIGURE 7: Double-jump refolding experiments for pelC. (a) The change in amplitude for the slowest phase of folding at various refolding delay times measured by fluorescence (○) or far-UV CD (●). (b) The change in amplitude of each observed kinetic phase at increasing refolding delay time determined by fluorescence for the 1.1 s (●), 21 s (▲), and 46 s phase (△). Conditions were 25 mM MES pH 6, 50 mM NaCl, 25 °C and residual gdn-HCl concentration of 0.4M.

amplitude of the 1.1-s phase decreases exponentially to a limiting value of about 0.4 (Figure 7b). However, the relative amplitudes of the two slower phases both increase exponentially with delay time to limiting values of 0.3 and 0.1. This is very strong evidence that there are multiple populations of unfolded protein molecules that interconvert relatively slowly. (The remaining relative amplitude, 0.2, is attributable to the 0.25-s phase, which is not resolved in the manual-mixing experiments.) Unfolding of pelC occurs very rapidly at 0 °C, pH 9.5, and in 5 M gdn-HCl (~25 s). Because of the high activation enthalpy, *cis*−*trans* isomerization of prolyl-peptide bonds will be dramatically slower. Thus, the equilibration of the *cis*−*trans* isomers will be very slow compared to unfolding, effectively decoupling these processes. This experiment allows one to observe the isomerization directly. The increase in amplitude as the protein is left unfolded for longer times before refolding results from more nonnative prolyl peptide bonds forming and more molecules populating the slow kinetic phases. The 1.1-s phase shows a decrease in amplitude because fewer pelC molecules are able to populate the fast-folding pathways.

Proline isomerization occurs with a characteristically high activation enthalpy (*45*). In model peptide systems, this is 19 ± 3 kcal/mol (*45, 49*). Using eq 2, the activation enthalpy can be calculated from the rate dependence on temperature in 0 M gdn-HCl. The slowest phase has $\Delta H^{\ddagger} = 21.2 \pm 0.9$ kcal/mol and $\Delta S^{\ddagger} = 5.8 \pm 0.2$ cal/mol K. This suggests that a typical proline isomerization event is responsible for the slow folding of this phase. For the intermediate slow phase $\Delta H^{\ddagger} = 16.0 \pm 0.7$ kcal/mol and $\Delta S^{\ddagger} = -11.2 \pm 2.5$ cal/mol K (determined with the P220A mutant as described in the following paper in this issue). These activation parameters are also typical of proline isomerization.

The enzyme peptidyl-prolyl isomerase has been shown to catalyze the *cis*−*trans* isomerization of X-Pro peptide bonds in small polypeptides and some proteins (*50*). The catalytic ability of this enzyme was tested on pelC. In a fluorescence experiment monitoring folding in 0.3 M urea, it was found that the rates of the slow phases are enhanced. For the slowest phase, the rate approximately doubles from 0.0070 to 0.0147 s^{-1}. The intermediate slow phase shows an almost 3-fold rate enhancement. The rate increases from 0.0301 to 0.0855 s^{-1} in the presence of 1 μM human PPI.

All of the presented data strongly support the proposal that the two slow steps in pelC folding are due to the *cis*−*trans* isomerization of prolyl-peptide bonds.

PelC CD Calculations. It was noted that when the folding kinetics are followed by near-UV CD, there is a change of sign in the fastest observed folding phase. This phase occurs with a rate constant that agrees, within experimental error, with that measured with far-UV CD. The experimental evidence so far cannot determine whether this species is nativelike or not. It was hypothesized that a portion of the folding protein has nativelike secondary structure, and this portion has a negative near-UV CD, in contrast to the overall positive CD of the native protein. To test this hypothesis, calculations on pelC with each individual tyrosine and tryptophan changed to alanine were carried out. The difference spectra between the wild-type and mutant proteins were then obtained. If an individual aromatic side chain or a cluster of aromatic side chains has a significant negative band in the near-UV, this might indicate which side chains were structured in the intermediate. The CD spectrum for native pelC was calculated in the near-UV spectrum. The calculation is in good agreement with experiment (Figure 8a). The experimental maximum is at 279 nm with an intensity of 174 deg cm^2/dmol. The calculation predicts the correct sign of the CD band with an intensity of 231 deg cm^2/dmol at 273 nm. Qualitatively, the features are also quite good. The tail above 290 nm is not predicted by the theory. However, we suspect that this results from disulfide bonds, which are not considered in the calculations.

Difference spectra were obtained in order to resolve individual aromatic side chain contributions to the CD spectrum. Figure 8b shows representative difference spectra for some of the mutations. (Difference CD spectra for all aromatics in both the near and far-UV are provided in the Supporting Information.) The difference spectra show the individual contributions to the near-UV CD. Most side chains make positive contributions, but several side chains make negative contributions to the spectrum. If one looks at only the residues in the β-helix region, one sees that the sum of the CD values at 277 nm is −8 deg cm^2/dmol (Table 2). This is consistent with the magnitude of the fast phase in the refolding process. The observed amplitude is −35 deg cm^2/dmol (Table 1). This supports, but does not prove, the hypothesis that the fastest phase in pelC folding results from

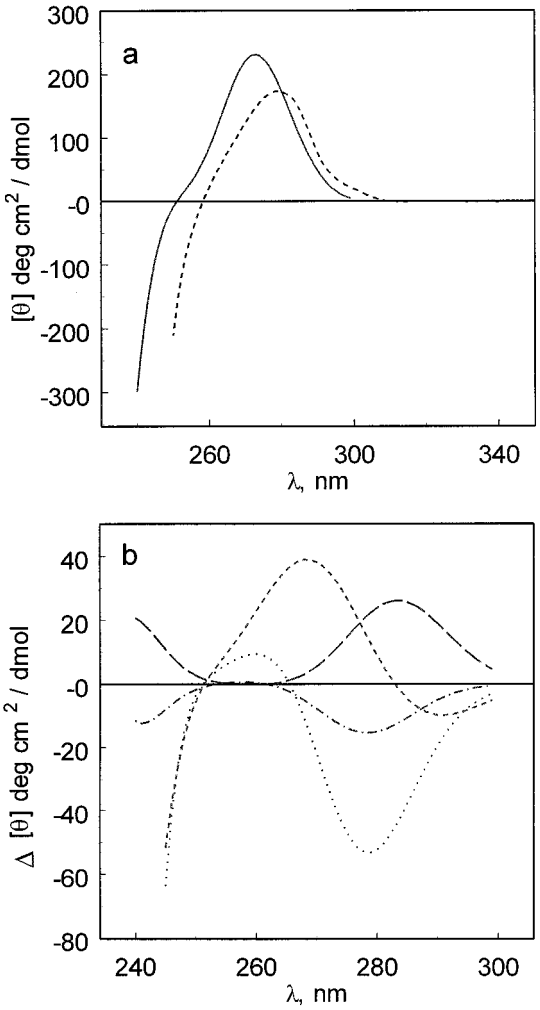

FIGURE 8: (a) Calculated near-UV CD spectrum (—) and experimental CD spectrum (- - -) for pelC. (b) Some representative difference CD spectra showing the individual contributions to the CD spectrum for W276 (···), W256 (- - -), Y184 (•-•-•), and Y230 (—).

Table 2: Calculated Near-UV CD for Aromatic Amino Acids in the β-Helix Region

residue no.	$[\theta]_{277}$ nm (deg cm^2/dmol)	residue no.	$[\theta]_{277}$ nm (deg cm^2/dmol)
W106	−11	Y207	6
W142	−1	Y211	0
W256	19	Y212	6
W276	−52	Y230	18
Y56	23	Y234	−1
Y184	−15	Total	−8

the rapid formation of the β-helix domain. In a single step, the β-sheet backbone forms, and at the same rate, the aromatic side chains in this region fold to their native structures. In a slower phase, the remainder of the side chains, which are in the loop regions of pelC, adopt their native conformations as the loop regions fold. A corresponding phase is not observed in the far-UV because the majority of the rest of the molecule is unordered structure and there is no detectable change in going from the dynamically unordered random coil to the statically unordered loops, i.e., this phase is spectroscopically silent in the far-UV CD.

It has also been shown (*51*) that, at pH 2 and NaCl concentrations greater than 100 mM, an intermediate is stabilized with a far-UV CD spectrum very similar to that of native pelC but a near-UV CD opposite in sign, with an intensity of about −60 deg cm^2/dmol at 280 nm (Figure 4b). The total side-chain contribution from the β-helix domain cannot account for this amplitude. There are some subsets of individual contributions that could account for the amplitude but no specific assignments are possible. It is likely that the kinetic and equilibrium intermediates are not as similar as originally thought. It is possible that binding of anions induces a conformation with only partial native structure and that some side chains might assume orientations different from those in native pelC.

DISCUSSION

The folding of small proteins is generally a relatively fast process, especially the formation of secondary structure (*1*−*3*). Secondary structure formation for many larger proteins occurs on a relatively fast time scale as well (*52*). In the folding of small and large proteins alike, the rate-limiting steps that occur on time scales on the order of tens of seconds or more may result in the formation of ordered secondary structure, but the energy barriers are due to a process other than secondary structure formation. In many cases, along with the added complexity of intramolecular domain association and subunit association, the slow steps of folding involve slow *cis*−*trans* isomerization of X-Pro peptide bonds (*45*−*48*). In larger proteins, retardation of protein folding by this isomerization is much more common. One reason is that large proteins contain more amino acids, and the statistical probability of prolines being present is greater. The presence and location of prolines are certainly not random occurrences. One of the specific roles of proline is to form a tight turn or kink in the backbone. Larger proteins often have highly evolved and optimized functions requiring finely tuned architecture. Proline side chains are very important in fine-tuning backbone architecture, and *cis* prolines are often functionally important.

In studying the folding mechanism of RNase A, Baldwin and co-workers (*53*−*55*) observed multiple unfolded populations corresponding to fast and slow folding kinetics. Brandts et al. (*45*) first proposed the proline isomerization hypothesis for RNase A, which states that the slow- and fast-folding forms of the protein differ in the *cis*−*trans* configuration of X-Pro peptide bonds. The original proposal suggested that the slow and fast folding forms of the protein exist in equilibrium and the slow form must convert to the fast form prior to folding to the native protein. It was subsequently shown that in RNase A, an intermediate is formed with some degree of compact structure but with some molecules having the incorrect proline conformation (*56*, *57*). This cleared up some problems with the original ideas. It seems unlikely that an entire protein could remain completely unfolded until one proline obtains its correct isomeric configuration. This leads to the view that a sizable fraction of the protein can acquire native structure while the local region about the incorrect proline isomer is somewhat unordered.

There are 12 prolines in pelC, and one of these, Pro 220, is in the *cis* conformation in the native enzyme. In model peptides and unordered proteins, the ratio of *trans*:*cis* isomers of proline is about 70:30 (*45*). The slow kinetics result from the slow interconversion of these isomers. The slowest kinetic

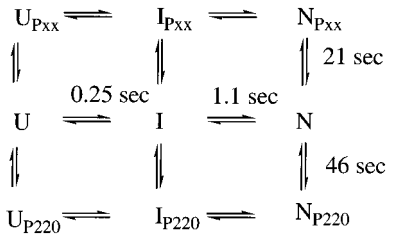

FIGURE 9: A model for the folding mechanism of pelC. U is the unfolded protein, I is the intermediate formed in the fast phase, and N is the native protein. N with a subscript represents a pseudo-native state in which the only major difference from the native protein is the conformation of a peptide bond. U, I, and N represent the major pathway taken when all peptide bonds are in the correct conformation. U_{P220}, I_{P220}, and N_{P220} represent the slowest pathway when Pro220 is in the *trans* conformation in the unfolded state. U_{Pxx}, I_{Pxx}, and N_{Pxx} is the pathway taken when other prolines are in the *cis* conformation in the unfolded state.

folding phase for pelC exhibits properties that are very typical of proline isomerization. These include a relaxation time of 46 s, a high activation enthalpy, catalysis by the enzyme PPI, and an increase in the amplitude of the slow phase with increasing time of unfolding during a double-jump assay. The intermediate slow phase shows similar properties. The relaxation time of 21 s and the increase in amplitude in the double-jump assay are consistent with proline isomerization, as is the 16.0 kcal/mol activation enthalpy and the catalysis by PPI.

Pro220 is a plausible candidate for a proline that is responsible for one of the slow phases (*30*). This residue is in the *cis* conformation in the native structure (*18*). It is located within the central β-helix region at the end of a strand. Results from site-directed mutagenesis indicate that isomerization of the Leu219−Pro220 peptide bond results in the slowest kinetic phase observed (*30*). In the mutant P220A, the 46-s kinetic phase is eliminated. It is also possible that prolines that are *trans* in the native protein demonstrate slow kinetics, because in the unfolded protein, some small population is *cis*. In pelC, the 21-s phase is not the result of isomerization of a native *cis* proline. Folding kinetics of P220A shows a slow phase that is consistent with the 21-s phase observed in wild-type pelC. Experiments with other proline→alanine/valine mutants indicate that no single prolyl-peptide bond is responsible for this phase (*30*). It is more likely that this phase results from an ensemble of prolines in the incorrect isomeric configuration. It is also possible that this phase results from isomerization of nonprolyl peptide bonds. This phenomenon has recently been observed by Pappenberger et al. (*58*).

A proposed kinetic model is presented in Figure 9, and can be described as follows for the case of folding with all of the prolines in the correct native configuration. The major fast phase results in the complete formation of the secondary structure. This occurs in a single cooperative step. At the same time, certain aromatic side chains of the molecule are forming a defined tertiary structure. The possibility of a population of molecules forming rapidly with completely native side-chain structure was ruled out by the negative amplitude in the fast phase of folding observed by near-UV CD. It is very possible that the side chains that are structured at the end of this phase are in an essentially native conformation. Calculations suggest that the aromatic side chains in the β-helix region make a negative contribution to the near-UV CD spectrum, which overall is positive. Also, at low pH and high salt, an intermediate with a negative CD amplitude in the near-UV is stable in pelC (Figure 4b). It is possible that these intermediate states are structurally related.

The next step in the folding process involves the ordering of the remainder of the side chains. These side chains are in the loop regions of pelC. Thus, because the backbone in the loop regions are dynamically unordered in the intermediate I and statically unordered in N, no changes in the far-UV CD are observed.

The case of folding with one or more prolines in the incorrect configuration is more complicated and is also represented in the kinetic model (Figure 9). When the unfolded protein solution is transferred to conditions stabilizing the native fold, there is a rapid condensation of the structure via at least three pathways. For the 46-s phase, the region around the incorrect proline is highly disordered because of the inability to form some native contacts. It seems unlikely that the proline isomerization is occurring in a completely unordered protein. It is more likely that the majority of the protein is folded correctly but the region of the protein near the incorrect proline isomer is unstructured or improperly folded. The 21-s phase occurs slightly faster, probably because structural constraints put strain on the incorrectly configured prolyl peptide bond, facilitating its conversion to the correct configuration. That is to say, the local environment of the polypeptide chain lowers the activation enthalpy, thus resulting in a slightly faster isomerization rate. This results in an activation enthalpy that approaches the lower limit observed for proline isomerization. It is also possible that an intermediate helps stabilize the correct backbone geometry. One commonly observed property of proline isomerization is the independence of the rate on denaturant concentration (*59*). This is not observed for pelC, but can be explained by our model. The presence of an intermediate strongly influences the rate of folding for pelC, and the intermediate's stability is strongly dependent on denaturant concentration. As the intermediate is destabilized, the rate dramatically slows, and only one phase is observed, corresponding to a rate-limiting proline isomerization.

In the presence of PPI, rate enhancements of about 2−3-fold are observed. PPI does not necessarily show dramatic rate enhancements or catalyze all prolyl isomerization events (*50*, *60*). There must be access for the enzyme active site to the improperly configured prolines. In the present case, access to the incorrect prolines is apparently limited. This observation is consistent with the proposed folding model. The formation of essentially all of the secondary structure occurs in about 0.25 s. This occurs in parallel with the formation of some degree of tertiary structure. It is therefore not surprising that the folded regions of pelC protect the incorrectly folded proline residues from PPI.

Individual Aromatic Side-Chain Contributions to the Near-UV CD. CD in the near-UV is much less predictable than that in the far-UV. In the far-UV the major chromophore is the peptide group. The predictability lies in the secondary structures that can be populated. In the near-UV the chromophores are primarily the side chains of tryptophan, tyrosine, and phenylalanine. These side chains can combine in all kinds of geometries and couple in an almost infinite variety of ways. Therefore, one cannot relate the sign, shape, or intensity of the CD spectrum to any particular structure.

However, one can look at particular contributions and changes to the near-UV CD spectrum with conditions.

The kinetic experiments indicate that some collapsed intermediate forms in the early stages of folding. This intermediate has a very nativelike secondary structure, but the tertiary structure is different from that of the native protein. At least that is what one might think at first. CD calculations support the idea that the β-helix region is the domain that forms in the fast kinetic phase. This domain forms rapidly in the folding process, followed by the slower arrangement of aromatic side chains in the loop regions of pelC. In a previous study (*26*) of the equilibrium denaturation of pelC, calorimetry indicated that two energetic domains were present with similar thermal stabilities. The nature of the two domains was not identified. It is possible that the β-helix region constitutes one of the domains observed in the equilibrium experiments, and the loop regions form the other domain. The two domains are not observed in unfolding experiments because they are interconnected. They can be resolved in the kinetic refolding experiments because of the sequential nature of the folding pathway. The formation of the β-helix domain must occur before the side chains in the loop regions are in close enough proximity to interact and form the minimum energy conformation.

Near-UV CD is a powerful and sensitive tool for observing the formation of side-chain structure during protein folding, but it has gone widely underutilized. This is possibly because far-UV CD overshadows the usefulness of near-UV CD. Different far-UV CD spectra are very characteristic of specific secondary structures and combinations thereof, and the rules governing this are quite well understood, but the only rules for CD in the near-UV are that aromatic side chains and disulfide bonds are the chromophores. There is no a priori way to tell from CD what the specific conformation of the side chain is. This study demonstrates the qualitative utility of near-UV CD in understanding a kinetic protein folding mechanism. It is not too surprising that there is a change of the sign of the folding amplitude. To our knowledge, this behavior has not previously been observed with near-UV CD, but similar observations have been made with far-UV CD (*44*, *61*−*63*). These, however, were overshoots of the native amplitude and not opposite in sign to the native CD.

The results presented in this paper demonstrate that the kinetic folding mechanism of pelC is overall rather simple. The formation of secondary structure occurs in a single cooperative step, along with some ordering of side chains. The remainder of the backbone and the side chains fold in a second step. The most complex part of the folding mechanism is well characterized and involves two proline isomerization steps. One of these slow phases is due to isomerization of Pro220 and the other is a result of the parallel isomerization of several other prolines. Systematic mutations of all of the proline residues in pelC have been carried out in order to understand more completely the slow folding kinetics of pelC. This study is presented in the following paper in this issue (*30*).

ACKNOWLEDGMENT

We would like to express our thanks to Professor Noel Keen for providing starter cultures of cloned pelC.

SUPPORTING INFORMATION AVAILABLE

Residual plots for far- and near-UV CD and fluorescence kinetic experiments are available. Calculated far- and near-UV CD spectra for pelC and difference spectra for all aromatic mutations are available. This material is available free of charge via the Internet at http://pubs.acs.org.

REFERENCES

1. Dill, K. A., and Chan, H. S. (1997) *Nat. Struct. Biol. 4*, 10−19.
2. Dinner, A. R., Šali, A., Smith, L. J., Dobson, C. M., and Karplus, M. (2000) *Trends Biochem. Sci. 25*, 331−339.
3. Dobson, C. M., Šali, A., and Karplus, M. (1998) *Angew. Chem., Int. Ed. 37*, 868−893.
4. Brockwell, D. J., Smith, D. A., and Radford, S. E. (2000) *Curr. Opin. Struct. Biol. 10*, 16−25.
5. Clarke, J., and Itzhaki, L. S. (1998) *Curr. Opin. Struct. Biol. 8*, 112−118.
6. Dobson, C. M., and Karplus, M. (1999) *Curr. Opin. Struct. Biol. 9*, 92−101.
7. Yeh, S. R., Takahashi, S., Fan, B., and Rousseau, D. L. (1997) *Nat. Struct. Biol. 4*, 51−56.
8. Chen, E., Wood, M. J., Fink, A. L., and Kliger, D. S. (1998) *Biochemistry 37*, 5589−5598.
9. Chan, C. K., Hu, Y., Takahashi, S., Rousseau, D. L., Eaton, W. A., and Hofrichter, J. (1997) *Proc. Natl. Acad. Sci. U.S.A. 94*, 1779−1784.
10. Akiyama, S., Takahashi, S., Ishimori, K., and Morishima, I. (2000) *Nat. Struct. Biol. 7*, 514−520.
11. Gruebele, M., Sabelko, J., Ballew, R., and Ervin, J. (1998) *Acc. Chem. Res 31*, 699−707.
12. Takahashi, S., Yeh, S. R., Das, T. K., Chan, C. K., Gottfried, D. S., and Rousseau, D. L. (1997) *Nat. Struct. Biol. 4*, 44−50.
13. Capaldi, A. P., and Radford, S. E. (1998) *Curr. Opin. Struct. Biol. 8*, 86−92.
14. Jackson, S. E., and Fersht, A. R. (1991) *Biochemistry 30*, 10428−10435.
15. Kuhlman, B., Boice, J. A., Fairman, R., and Raleigh, D. P. (1998) *Biochemistry 37*, 1025−1032.
16. Kuhlman, B., Luisi, D. L., Evans, P. A., and Raleigh, D. P. (1998) *J. Mol. Biol. 284*, 1661−1670.
17. Yoder, M. D., Lietzke, S. E., and Jurnak, F. (1993) *Structure 1*, 241−251.
18. Yoder, M. D., Keen, N. T., and Jurnak, F. (1993) *Science 260*, 1503−1507.
19. Betts, S., and King, J. (1999) *Structure 7*, R131−R139.
20. Haase-Pettingell, C., and King, J. (1997) *J. Mol. Biol. 267*, 88−102.
21. King, J., Haase-Pettingell, C., Robinson, A. S., Speed, M., and Mitraki, A. (1996) *FASEB J. 10*, 57−66.
22. Robinson, A. S., and King, J. (1997) *Nat. Struct. Biol. 4*, 450−455.
23. Fuchs, A., Seiderer, C., and Seckler, R. (1991) *Biochemistry 30*, 6598−6604.
24. Miller, S., Schuler, B., and Seckler, R. (1998) *Biochemistry 37*, 9160−9168.
25. Lazo, N. D., and Downing, D. T. (1998) *Biochemistry 37*, 1731−1735.
26. Kamen, D. E., Griko, Y., and Woody, R. W. (2000) *Biochemistry 39*, 15932−15943.
27. Press, W. H., Flannery, B. P., Teukolsky, S. A., and Vetterling, W. T. (1989) *Numerical Recipes: The Art of Scientific Computing (FORTRAN Edition)*, pp 523−528, Cambridge University Press, Cambridge, U.K.
28. Kuwajima, K., Hiraoka, Y., Ikeguchi, M., and Sugai, S. (1985) *Biochemistry 24*, 874−881.
29. Eyring, H. (1935) *Chem. Rev. 17*, 65−77.
30. Kamen, D. E., and Woody, R. W. (2002) *Biochemistry 41*, 4724−4732.
31. Woody, R. W., and Sreerama, N. (1999) *J. Chem. Phys. 111*, 2844−2845.

32. Bayley, P. M., Nielsen, E. B., and Schellman, J. A. (1969) *J. Phys. Chem. 73*, 228−243.
33. Goux, W. J., and Hooker, T. M. (1980) *J. Am. Chem. Soc. 102*, 7080−7087.
34. Clark, L. B. (1995) *J. Am. Chem. Soc. 117*, 7974−7986.
35. Ridley, J., and Zerner, M. C. (1973) *Theor. Chim. Acta 32*, 111−134.
36. Woody, R. W. (1968) *J. Chem. Phys. 49*, 4797−4806.
37. Grishina, I. B., and Woody, R. W. (1994) *Faraday Discuss. 99*, 245−262.
38. Matouschek, A., Otzen, D. E., Itzhaki, L. S., Jackson, S. E., and Fersht, A. R. (1995) *Biochemistry 34*, 13656−13662.
39. Oliveberg, M. (1998) *Acc. Chem. Res. 31*, 765−772.
40. Otzen, D. E., Kristensen, O., Proctor, M., and Oliveberg, M. (1999) *Biochemistry 38*, 6499−6511.
41. Silow, M., and Oliveberg, M. (1997) *Biochemistry 36*, 7633−7637.
42. Sosnick, T. R., Shtilerman, M. D., Mayne, L., and Englander, S. W. (1997) *Proc. Natl. Acad. Sci. U.S.A. 94*, 8545−8550.
43. Danner, M., Seckler, R. (1993) *Protein Sci. 2*, 1869−1881
44. Matagne, A., Jamin, M., Chung, E. W., Robinson, C. V., Radford, S. E., and Dobson, C. M. (2000) *J. Mol. Biol. 297*, 193-210.
45. Brandts, J. F., Halvorson, H. R., and Brennan, M. (1975) *Biochemistry 14*, 4953−4963.
46. Hurle, M. R., and Matthews, C. R. (1987) *Biochim Biophys Acta 913*, 179−184.
47. Kiefhaber, T., Quaas, R., Hahn, U., and Schmid, F. X. (1990) *Biochemistry 29*, 3053−3061.
48. Schmid, F. X., and Baldwin, R. L. (1978) *Proc. Natl. Acad. Sci. U.S.A. 75*, 4764−4768.
49. Cheng, H. N., and Bovey, F. A. (1977) *Biopolymers 16*, 1465−1472.
50. Lang, K., Schmid, F. X., and Fischer, G. (1987) *Nature 329*, 268−270.
51. Kamen, D. E., and Woody, R. W. (2001) *Protein Sci. 10*, 2123-2130.
52. Jaenicke, R. (1987) *Prog. Biophys. Mol. Biol. 49*, 117−237.
53. Garel, J. R., and Baldwin, R. L. (1973) *Proc. Natl. Acad. Sci. U.S.A. 70*, 3347−3351.
54. Garel, J. R., and Baldwin, R. L. (1975) *J. Mol. Biol. 94*, 611−620.
55. Garel, J. R., Nall, B. T., and Baldwin, R. L. (1976) *Proc. Natl. Acad. Sci. U.S.A. 73*, 1853−1857.
56. Nall, B. T., Garel, J. R., and Baldwin, R. L. (1978) *J. Mol. Biol. 118*, 317−330.
57. Schmid, F. X., and Baldwin, R. L. (1979) *J. Mol. Biol. 135*, 199−215.
58. Pappenberger, G., Aygun, H., Engels, J. W., Reimer, U., Fischer, G., and Kiefhaber, T. (2001) *Nat. Struct. Biol. 8*, 452−458.
59. Schmid, F. X., and Baldwin, R. L. (1979) *J. Mol. Biol. 133*, 285−287.
60. Jackson, S. E., and Fersht, A. R. (1991) *Biochemistry 30*, 10436−10443.
61. Clarke, D. T., Doig, A. J., Stapley, B. J., and Jones, G. R. (1999) *Proc. Natl. Acad. Sci. U.S.A. 96*, 7232−7237.
62. Matagne, A., Chung, E. W., Ball, L. J., Radford, S. E., Robinson, C. V., and Dobson, C. M. (1998) *J. Mol. Biol. 277*, 997−1005.
63. Radford, S. E., Dobson, C. M., and Evans, P. A. (1992) *Nature 358*, 302−307.
64. Sayle, R. A., and Milner-White, E. J. (1995) *Trends Biochem. Sci. 20*, 374−376.

BI0115129